Adsorption-induced swelling impact on CO 2 transport in kerogen microporosity as described by free volume theory

Kristina Ariskina, Guillaume Galliéro, Amaël Obliger

Adsorption-induced swelling impact on CO_2 transport in kerogen microporosity as described by free volume theory

Kristina Ariskina,[†] Guillaume Galliéro,[†] and Amaël Obliger[*,‡]

[†]*Laboratoire des Fluides Complexes et leurs Réservoirs, Univ. of Pau and Pays de l'Adour/CNRS/TOTAL/E2S, UMR 5150 Pau 64000, France*

[‡]*Institut des Sciences Moléculaires, Univ. of Bordeaux, CNRS, UMR 5255, Talence 33405, France*

E-mail: amael.obliger@u-bordeaux.fr

Abstract

In order to examine the impact of the flexibility of kerogens' microporosity on the transport of adsorbed CO_2, we develop a free volume model that notably accounts for adsorption-induced swelling exhibited by flexible kerogen structures. We first show that, for CO_2 compared to CH_4 at constant fluid molar loading and in the same conditions, the atomistic model of microporous kerogen we use exhibits slightly less swelling upon adsorption. This swelling comes with an increase in the free volume accessible to the CO_2 molecules, which can then diffuse faster when the fluid loading increases, without introducing significant collective effects on the transport properties. Consequently, transport can be considered diffusive and the self-diffusion coefficient can be used as a proxy for the collective diffusion (or transport) coefficient. Finally, as previously demonstrated for CH_4, a free volume model based on the Fujita–Kishimoto theory describes the transport enhancement with CO_2 fluid loading. Although CO_2 interacts

more strongly than CH_4, the parameters of the free volume models for both fluids are shown to be similar. Together with the diffusive nature of transport, it suggests an even broader applicability of the model to the transport of light alkanes and mixtures, thus greatly simplifying transport modeling for geological applications such as carbon sequestration in shales.

Introduction

Intensive combustion of petroleum and coals since the pre-industrial period has determined the global picture of atmospheric pollution. Overall, the concentration of CO_2, for instance, has been reported increased in 40 %.[1] A possible way to mitigate unfavorable emissions of CO_2 risen into the atmosphere is their geological sequestration in the microporosity (pore size below 2 nm) of organic matter (OM). Furthermore, CO_2 injection could greatly contribute to the enhancement of hydrocarbon recovery from unconventional reservoirs, such as shales.[2]

The presence of microscopic scale pores leading to a large surface-to-volume ratio has predetermined the vast use of kerogen, the largest pool of OM of shales, as a promising storage material for CO2. The large variety of kerogens present in nature induces a great complexity in accounting for their diverse physical-chemical and mechanical properties – chemical composition, ultra-low porosity, internal flexibility, structural heterogeneity, etc. This should be accounted for in investigations of transport and adsorption which are the key processes controlling the success of sequestration of CO_2 within shales' organic matter. However, mechanisms happening at larger scales, such as fluid slippage, wettability, or Knudsen diffusion are important as well.[3–14]

The construction of atomistic kerogen models[15–19] has led to several pioneering works on adsorption and diffusion done by classical molecular dynamics (MD), which have been covered in recent comprehensive reviews.[20,21] The majority of molecular investigations have been performed for fluid adsorption,[22–32] although transport within the ultra-confining and amorphous network of kerogens' micropores has been addressed, but mostly by neglecting the

viscoelastic nature of the kerogens' microstructures, which possibly leads to non negligible poroelastic couplings between the dynamics of the fluid and microstructure and significant adsorption-induced swelling. Most of the MD studies of transport and diffusion in kerogens microporosity were performed by considering the microstructures as rigid.[7,15,33–43] Due to the increase of volume occupied by fluid upon adsorption while the pore space remains constant, transport properties decerase with fluid loading as the free volume required for the molecules to diffuse diminishes. Only few recent studies have considered fully the impact of adsorption-induced swelling on transport properties in kerogen.[44,45] They have shown for methane adsorbed in a viscoelastic kerogen microstructure that adsorption capacity increases due to inherent flexibility of kerogen and the accompanying adsorption-induced swelling phenomena lead to accelerated diffusion of fluid molecules. The impact of pore size fluctuations caused by the solid's flexibility and the mobility of local structural networks on the nature of the transport has shown to play an important role in the diffusion mechanisms. Furthermore, despite the significant change in pores' shape and improvement in pore connectivity due to CH_4 adsorption-induced swelling, fluid-fluid cross-correlations remain negligible and transport can be considered diffusive, as for rigidified kerogens' microstructures.

Although carbon sequestration in shales is an important topic, transport of CO_2 in atomistic microporous kerogen models has been scarcely addressed using MD simulations.[46,47] For a molecular model of type II kerogen considered rigid in the simulations, it has been noticed that the self-diffusion coefficient of CO_2 decreases with fluid loading.[46,47] Additionaly, those studies have pointed out that CH_4 diffusion is larger due to the difference in isosteric heat of adsorption between these fluids.

In contrast to these studies, we study the transport properties of CO_2 adsorbed in an atomistic model of kerogen's microstructure, which exhibits important swelling upon adsorption, while fully accounting for the flexibility effects of the microstructure on the dynamics of the fluid during the MD calculations. After quantifying adsorption-induced swelling and its impact on the pore space accessible to the CO_2 molecules, we investigate the impact

of collective effects on transport, and we propose a model based on the Fujita-Kishimoto free volume theory[48–52] to capture the increasing trend of the diffusion coefficient with fluid loading for thermophysical conditions relevant for CO_2 geological sequestration.

This paper is organized as follows. First, the influence of CO_2 adsorption on the pore space is discussed. Then, swelling-based diffusion is investigated, incorporating the poroelastic coupling between the kerogen matrix and the fluid on the collective effects of transport. In addition, the small anisotropy effect related to the kerogen matrix is assessed. At last, the free volume model is applied to capture the solid-fluid coupling impacting transport and its parameters are discussed.

Methods

Kerogen Microstructure Model

The used model of microporous kerogen has been constructed by liquid quench MD, which is thoroughly described in.[19] It counts 16864 atoms with a H/C ratio of 1.1, corresponding to a type I kerogen in the middle of the oil formation window. Heteroatoms such as sulfur, oxygen, and nitrogen are not included in the matrix, as we believe they do not strongly affect transport. A closer look at the molecular model's chemical structure indicates that it is mostly made up of short aliphatic chains with 5 C atoms on average and small aromatic ring clusters with 10 C atoms on average, with an intermediate ring/chain ratio of 0.7. Because of the inclusion of elements that contribute to the stiffening (ring clusters) and softening (aliphatic chains) of the structure, this results in a "semi-flexible" matrix. Thus, its bulk modulus is moderate ($\simeq$ 1-5 GPa), as expected of immature kerogens. The bulk modulus of the matrix decreases with decreasing pressure P, increasing temperature T, and decreasing fluid loading w expressed in mg of fluid per g of matrix for geological conditions. We emphasize that the *mechanical* pressure applied to the system corresponds to the lithostatic pressure rather than any bulk fluid pressure. In shales, geology imposes mechanical pressure,

and fluid loading is determined by geological history, i.e. how many hydrocarbons were produced during maturation and how much of them were expelled. As a result, as in,[19] we treat pressure and fluid loading as independent variables.

Molecular dynamics setup

Interactions between the solid's atoms are described with the Adaptive Intermolecular Reactive Empirical Bond Order (AIREBO) potential, a well-proven force field for carbon and hydrogen, in order to accurately reflect the mechanical properties of the matrix. We use a modified version of the AIREBO potential where the long-range interactions have been slightly reparametrized.[19] The Elementary Physical Model (EPM) all-atoms potential proposed by Harris and Yung[53] has been used for the CO_2 molecules. The EPM model combines a rigid representation of the CO_2 molecules with Lennard-Jones and Coulombic interactions. The Lorentz-Berthelot combining rules have been used for the fluid-fluid and solid-fluid interactions.

The systems investigated, which include the microstructure and the fluid adsorbed inside, were first created by (i) reemploying the configurations already equilibrated at constant temperature and pressure from[44] for CH_4, where those molecules have all been replaced by CO_2 ones, and (ii) relaxing them at constant temperature and pressure in the isothermal-isobaric (NPT) ensemble to account for the kerogen matrix reorganization according to the substituted fluid. Then, the trajectories have been produced by MD calculations in the canonical (NVT) ensemble. The MD calculations have been done by applying three-dimensional periodic boundary conditions using LAMMPS with a timestep of 0.25 fs. Following,[54] the temperature and pressure have been controlled by the Nosé-Hoover thermostat and barostat with damping parameters of 0.1 and 0.4 ps, respectively. The constant volumes enforced during the MD trajectories in the NVT ensemble at various conditions (temperature, pressure, loading) come from the results obtained from the NPT calculations. The NPT simulations have been run for a total of several tens of ns, up to 70 ns for the lowest fluid loading. The

density change over the simulation time and its equilibrium fluctuations are provided in the Supplementary information.

Kerogen's Pore Volume Characterization Upon Adsorption

The kerogen's pore volume properties, the porosity and the free volume ratio, are computed from equilibrated configurations related to various temperature, pressure, and adsorption conditions with the same methods used in.[19] We briefly recall them here.

The porosity is computed by taking into account dimensionless points (50000 to reach convergence) that are randomly placed in the simulation box. The ratio of the number of points outside the atoms of the kerogen matrix against the total number of points gives the porosity, or the free volume ratio if we also discard the points inside the fluid molecules. The carbon and hydrogen atoms are considered spheres with diameters of 3.36 and 2.42 Å, respectively, using Lennard-Jones parameters from the modified AIREBO potential in this work. The volumetric swelling is simply calculated by comparing the volume of the fluid-containing matrix with that of the empty matrix at the same temperature and pressure.

For the accessible versions of the free volume ratio and porosity, 2.5 10^5 spheres with a diameter of 3.3 and 3.8 Å for CO_2 and CH_4 molecules, respectively, corresponding to their kinetic diameters,[55] that do not overlap with kerogen's atoms, are first created. If anything is specified, the CO_2 probe has been used. The accessible porosity is then obtained from the fraction of random points inside this set of spheres, and the accessible free volume ratio is obtained by subtracting the volume of the adsorbed CO_2 molecules. Given that CO_2 has a lower kinetic diameter than CH_4 and that oxygen interacts much more strongly than hydrogen with the kerogen's atoms, one can immediately note that CO_2 is by far an energetically denser fluid than CH_4. The accessible porous properties of the kerogen obtained using the CH_4 molecule as a probe and their application to the free volume model of transport are presented in the Supplementary Information.

Diffusion Coefficients Evaluation

Recently, it has been shown in[33–35] that the steady-state transport properties of fluids adsorbed in kerogen microstructures can be determined through equilibrium MD calculations by obtaining the collective diffusion coefficient. The self-diffusion coefficient D_s of a fluid molecule in the reference frame of the kerogen can be evaluated by observing the linear regime of the Mean Square Displacement (MSD) $\langle \Delta x^2(t) \rangle$ in one of the three dimensions, that is reached after a sufficiently long time, from

$$\langle \Delta x^2(t) \rangle = 2D_\mathrm{s}\, t + A, \tag{1}$$

where the brackets denote the ensemble averaging. The MSD is averaged over each adsorbed molecule, and a sliding average is performed along the trajectories. Additionally, the collective diffusion coefficient D_c can be determined by considering the MSD of the fluid center of mass ($x_\mathrm{c} = \sum_{i=1}^{N} x_i/N$ for pure fluids) via

$$\langle \Delta x_\mathrm{c}^2(t) \rangle = 2\frac{D_\mathrm{c}}{N}\, t + B, \tag{2}$$

where N is the number of fluid molecules.

Those two diffusion coefficients in fact differ from the total contribution of the cross-correlations between molecules to the transport coefficient because we have

$$D_\mathrm{c} = D_\mathrm{s} - \lim_{t\to+\infty} \frac{1}{Nt} \sum_{k\neq l} \langle x_k(t) x_l(0) \rangle \tag{3}$$

from the definition of the fluid c.o.m. and the long-time limits of Eqs. 1 and 2.

A few hundred or thousand ps to 10 or 50 ns, respectively, are common ranges for the linear fits used to calculate the self- and collective diffusion coefficients. For each condition, the error bars are estimated from 5 separate simulations. Their initial configurations have been taken from the NPT trajectories with a time interval of 500 ps between each.

Results and Discussions

Volumetric Expansion of Kerogen Upon CO_2 Adsorption

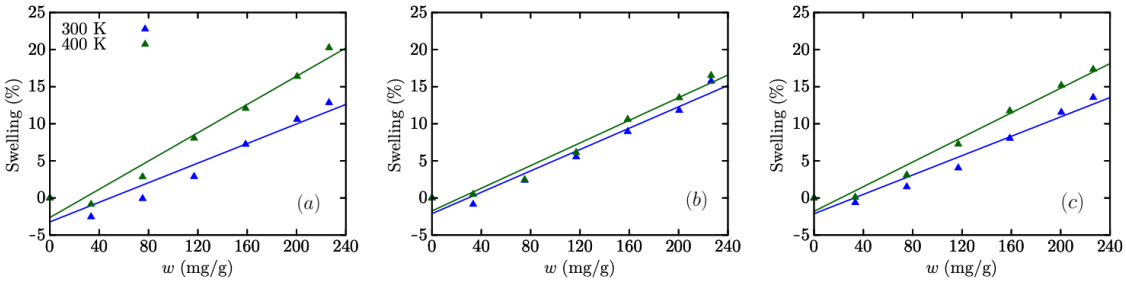

Figure 1: Evolution of the volumetric swelling due to CO_2 adsorption as a function of fluid loading w, expressed in milligram of fluid per gram of the kerogen matrix, at 300 and 400 K, and pressures of (a) 0.1 MPa, (b) 25 MPa, and (c) 100 MPa. The solid curves stand for linear models of swelling evolution.

The flexible kerogen matrix exhibits significant swelling due to the adsorption of CO_2, as shown in figure 1. The maximum volumetric expansion in the investigated conditions reaches slightly more than 20 % (400 K, 0.1 MPa). Nevertheless, there is no expansion of the matrix at ultra-low loading, the kerogen matrix even shrinks a little at 0.1 MPa or at larger pressures, but only at 300 K. Under the thermodynamic conditions investigated here and for the same molar loadings, shrinkage has not been observed for CH_4 [45] and adsorption-induced swelling is always larger for CH_4 than CO_2 (See Fig. 5 of SI). We conclude that shrinkage induced by CO_2 adsorption is due to the energetic density of CO_2, i.e., when the pore volume is low, as is the amount of adsorbed molecules, the fluid-solid interactions are then attractive and very strong. However, at higher pressures, the pore volume is so small that those interactions become more repulsive, and the kerogen matrix tends to be stiffer when denser, [19] thus becoming less prone to volume changes. Another anomaly occurs at moderate applied mechanical pressure, where at both temperatures swelling remains similar. The reduced difference in thermal expansion of the kerogen at 25 MPa might be caused by negative mechanisms, such as those potentially induced by the adsorption of an energetically dense fluid, but which nonetheless do not have a great impact on the qualitative characteristics of

the kerogen models.

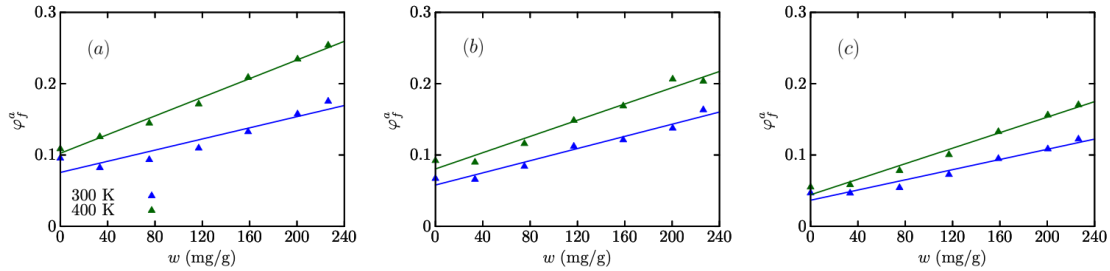

Figure 2: Evolution of the accessible free volume ratio with the CO_2 loading for the three different temperatures at pressures of (a) 0.1 MPa, (b) 25 MPa, (c) 100 MPa. The solid curves stand for linear models of the accessible free volume.

This adsorption-induced swelling is accompanied by an increase in the accessible free volume ratio following the same trends (figure 2). In contrast, the free volume ratio (see SI) can decrease with adsorption even at intermediate loadings ($40 \leq w \leq 160$ mg/g) and only slightly increases at higher loadings. Because the pore space into which fluid molecules cannot adsorb is not discarded when computing the free volume ratio, adsorption-induced swelling of CO_2 mostly increases the ratio of pore space that can be occupied by the fluid at the expense of the ratio of pore space where molecules cannot adsorb.

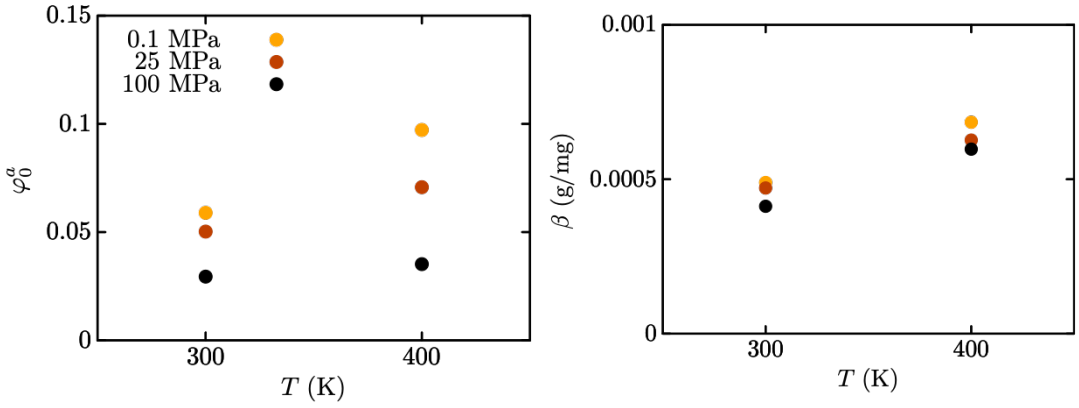

Figure 3: Accessible free volume without fluid adsorbed φ_0^a (left) computed with the probe of CO_2 and the linearity coefficient β (right) for a wide range of T-P conditions.

Finally, we deduce linear trends for the evolution of the accessible free volume ratio with

the fluid loading as

$$\varphi_f^a(w) = \varphi_0^a + \beta w, \tag{4}$$

where the constants φ_0^a and β are fitted against the data shown in fig. 2. Despite the fact that the weak shrinkage at very low loading is not captured, the evolution is quantitatively well captured when more fluid is absorbed, which corresponds to the most interesting conditions to examine transport properties. Values of φ_0^a and β are reported in Fig. 3, where we see that the accessible free volume ratio at infinitely low fluid loading barely increases with temperature for the largest mechanical pressure while clearly increasing for lower pressures. However, the constant β that captures the impact of adsorption-induced swelling on the accessible free volume increases with temperature while being quite insensitive to pressure. We now investigate the consequences of adsorption-induced swelling on transport.

Collective Effects on CO_2 Transport

In our earlier work[45] we have proven that the viscoelasticity of the kerogen has only negligible effects on the nature of the transport of adsorbed CH_4, i.e., transport is still diffusive as it would be if the kerogens' matrices are considered rigid.[33,35] In order to check that for CO_2, for which stronger fluid-solid interactions could promote internal fluid cross-correlations and thus collective effects on transport, the self- and collective diffusion coefficients have been compared. Their evolution with adsorbed fluid is shown in figure 4 for conditions close to typical geological ones, at temperatures of 300 K and 400 K and a mechanical pressure of 25 MPa. We immediately see that despite some large error bars (95% confidence intervals), especially at high fluid loadings and at 400K, the values of both diffusion coefficients remain close. Because the difference between those diffusion coefficients represents the long-term influence of the fluid's internal cross-correlations on transport, as seen from Eq. 3, we conclude that collective effects on CO_2 transport are negligible and we focus on the self-diffusion

coefficient to investigate the transport properties. Not only do strong solid-fluid interactions not induce persistent cross-correlations on fluid transport, that would be promoted by the kerogen's flexibility, but neither do stronger quadrupolar fluid-fluid interactions.

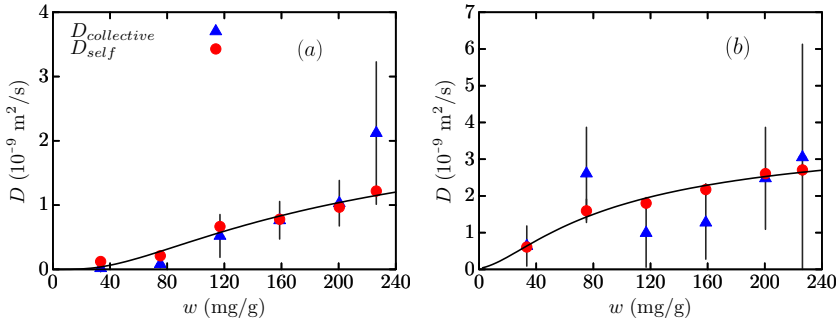

Figure 4: Self- and collective diffusion coefficients as a function of carbon dioxide loading for temperatures of (a) 300 K and (b) 400 K and a pressure of 25 MPa.

Diffusion Behavior With Fluid Loading

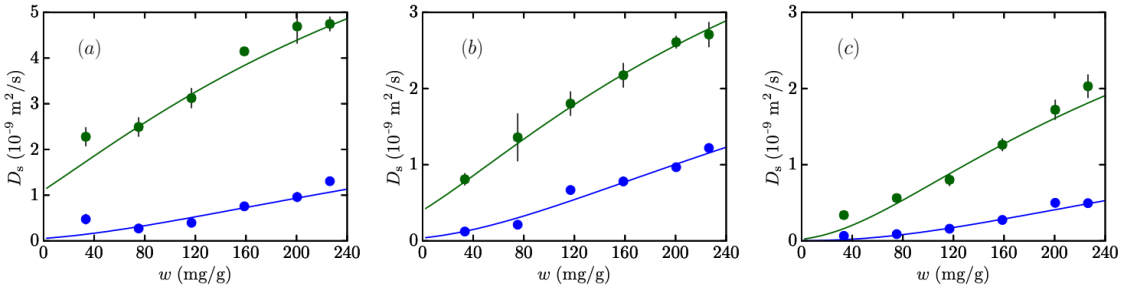

Figure 5: Evolution of the self-diffusion coefficient with the CO_2 loading for pressures of (a) 0.1, (b) 25, and (c) 100 MPa, at 300 (blue) and 400 K (green). The solid curves correspond to the free volume model for which the parameters $\alpha(T, P)$ and $\xi(T, P)$ are estimated from a best fit procedure and collected in figure 6. For ultra-confining pressure of 100 MPa, one of the fifth curves has been eliminated in an algebraic averaging procedure to obtain the proper average fitting curve.

As for CH_4,[45] although to a lesser extent, CO_2 diffusion increases with fluid loading due to adsorption-induced swelling. This is however better described by looking at the self-diffusion coefficient, which can be evaluated more easily than the collective one with respect to the statistics needed for accuracy. Before going further, we checked that anisotropy does not have a significant impact on CO_2 diffusion in this kerogen microstructure, as for CH_4.[45] Diffusion

is larger in one direction, but the ratio between the diffusivity in that direction and the average over the two others, which remain very similar, is always smaller than two and stays roughly constant with fluid loading (see SI). Because of that, we consider the average over the three directions to investigate the impact of adsorption-induced swelling on transport. Figure 5 displays the evolution of the self-diffusion coefficient with fluid loading for three different pressures, 0.1, 25, and 100 MPa, at both temperatures, 300 and 400 K. Except for low fluid loading at 0.1 MPa and 300 K, diffusion always increases with fluid loading, following the overall trend of the accessible free volume ratio. This correlation between diffusion and accessible pore space is thus not perfect, as the only decrease of the accessible free volume ratio with fluid loading reflected on the self-diffusion coefficient occurs for the most important decrease (0.1 MPa, 300 K). We now seek to develop a free volume model to capture the overall diffusion enhancement with fluid loading due to adsorption-induced swelling.

Free Volume Modeling

Because the accessible free volume ratio correlates very well with the self-diffusion coefficient under adsorption-induced swelling, we employ the Fujita-Kishimoto free volume theory relating the transport coefficient $D(w)$ to the fluid loading w through the accessible free volume ratio $\varphi_f^a(w)$ as

$$D(w) = \frac{k_B T}{\xi_0} \exp\left[\alpha \frac{\varphi_f^a(w) - \varphi_0^a}{\varphi_0^a \varphi_f^a(w)}\right], \tag{5}$$

where the pre-exponential factor, which includes the friction coefficient ξ_0, denotes the diffusivity at infinite dilution and the free volume parameter α characterizes the exponential increase with the accesible free volume. We only retain the overall linear increase in accessible

free volume ratio with fluid loading so that our free volume model

$$D(w) = \frac{k_B T}{\xi_0} \exp\left[\frac{\alpha}{\varphi_0^a} \frac{\beta w}{\varphi_0^a + \beta w}\right], \tag{6}$$

combining Eqs. 4 and 5, simply requires 4 constant parameters, ξ_0, α, β, and φ_0^a, where the values of the 2 latters as functions of the temperature and mechanical pressure are already known (Fig. 3).

The two other parameters, α and ξ_0, are then fitted against the diffusion coefficients, and the resulting trends of the free volume model (Eq. 6) are shown in Fig. 5, confirming that it captures well the impact of adsorption-induced swelling on diffusion, especially at the intermediate pressure of 25 MPa. Though we note that for the lowest and highest mechanical pressures considered (0.1 and 100 MPa) at 400 K, the model tends to underestimate diffusion. It also happens at 0.1 MPA and 300 K, where diffusion is not monotonic with fluid loading, but this is expected as shrinkage upon adsorption is more pronounced on the accessible free volume ratio and only its increase is considered in the linear model (Eq. 4).

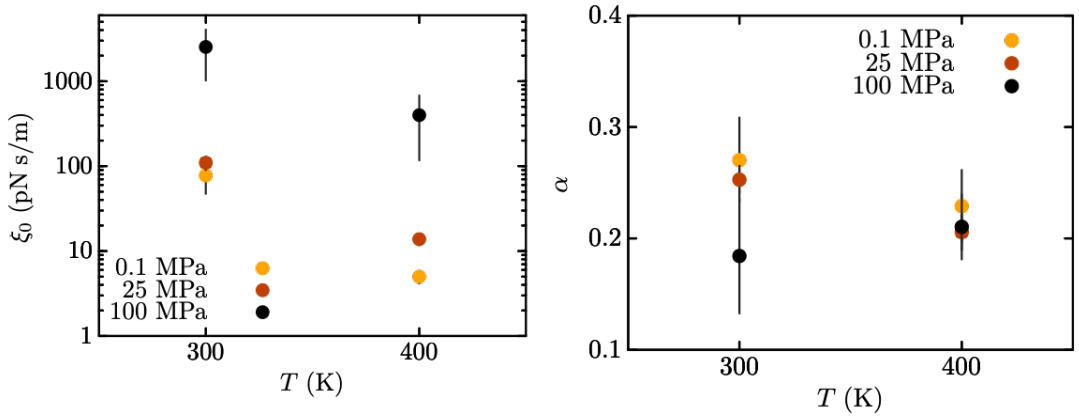

Figure 6: Friction coefficient ξ_0 (left) and the free volume parameter α (right) obtained from a fit procedure with the parameters φ_0^a and β corresponding to the different conditions taken from figure 3 with the CO_2 probe.

Going further, we investigate the behaviors of the parameters ξ_0 and α, for which their values have been gathered in Fig. 6 at all conditions investigated. We clearly see an increase

in the friction coefficient with mechanical pressure, which is moderate between 0.1 and 25 MPa but can reach an order of magnitude when going at 100 MPa. Such a significant variation is observed on the decrease of ξ_0 when temperature increases from 300 to 400 K. Finally, the behavior of the friction coefficient simply follows the swelling's variations with temperature and pressure. However, the free volume parameter α is not subject to important evolutions, especially at 400 K, where its values remain close at all three pressures. It is also the case at 300 K if we exclude the largest pressure, for which a large error bar is also observed. Furthermore, this condition is far from being realistic from a geological point of view and corresponds to the most severe case of confinement. Similar conclusions can be drawn if we use CH_4 as a probe for the estimation of the accessible free volume (see SI), which assesses the robustness of the free volume model used here.

Despite the stronger energetic density of CO_2 compared to CH_4, which yields slightly less swelling at same fluid molar loadings, diffusion is very similar for the two adsorbed fluids. Diffusion coefficients from[45] for CH_4 are gathered in the SI with those of CO_2 for comparison. As the same free volume model has also been successfully applied to CH_4[45] adsorbed in the same kerogen matrix, we can compare the parameters ξ_0 and α for both fluids to conclude that the stronger fluid-solid interaction of CO_2 lead to slightly larger values for the friction coefficient in the zero loading limit and to even smaller variations of the free volume parameter α while keeping very similar values for the two fluids.

Conclusions

We confirm that adsorption-induced swelling is important in the transport properties of kerogen microstructures that are not mechanically rigid, especially for CO_2 which strongly interacts with the matrix. As a result, the transport properties increase with fluid loading rather than decrease, as is the case of kerogen matrices that does not deform upon adsorption. CO_2 transport can be said to be purely diffusive in a flexible kerogen microstructure. As

for CH_4, kerogen's flexibility does not lead to significant collective effects on transport for CO_2 that can be considered purely diffusive, despite that it is an energetically denser fluid. This suggests that, even in the cases of CH_4/CO_2 mixtures, possibly involving light alkanes, no important cross-correlation would arise on transport properties between molecules of the same species and between molecules of different species, as already shown for linear alkanes' mixtures in rigidified kerogen models.[35] Meaning that, the sole impact of other components on transport of one species would happen through their influence on its accessible free volume within the swellable microstructure, which would be adequately quantified by their self-diffusion coefficients.

Focusing on capturing the trends of the self-diffusion coefficient with fluid loading demonstrates once again that the accessible free volume is the key quantity to model transport in kerogen's microporosity. The presented free volume model captures the dependence of transport of CO_2 on fluid loading for a carbon matrix that displays important adsorption-induced swelling for a broad set of thermophysical conditions, suggesting the wide applicability of the model for geological applications. While considering only linear increases of the accessible free volume into the model, the diffusion enhancement with fluid loading is controlled by a free volume parameter that does not significantly change with temperature and pressure, and remain close to what has been evaluated for methane in conditions relevant for carbon sequestration. We can postulate that this statement is accurate for light alkanes.

It implies that transport modeling in kerogen for such an application could be simplified, even in the case where kerogens' microporosity exhibits significant adsorption-induced swelling. Comparison with CH_4 indicates that, despite the contrast between both fluids, adsorption-induced swelling behavior is very similar at the same molar fluid loadings. This holds true as well for the impact on their transport properties. Then, the next challenge in modeling the transport properties of mixtures in swellable kerogen would be to predict the impact of co-adsorption on the free volume accessible to the mixtures' species.

References

(1) Yu, Z.; Griffis, T. J.; Baker, J. M. Warming temperatures lead to reduced summer carbon sequestration in the U.S. Corn Belt. *Communications Earth and Environment* **2021**, *2*, 1–11.

(2) Wang, S.; Yao, X.; Feng, Q.; Javadpour, F.; Yang, Y.; Xue, Q.; Li, X. Molecular insights into carbon dioxide enhanced multi-component shale gas recovery and its sequestration in realistic kerogen. *Chemical Engineering Journal* **2021**, *425*, 130292.

(3) Apostolopoulou, M.; Day, R.; Hull, R.; Stamatakis, M.; Striolo, A. A kinetic Monte Carlo approach to study fluid transport in pore networks. *The Journal of Chemical Physics* **2017**, *147*, 134703.

(4) Ning, Y.; Jiang, Y.; lin Liu, H.; Qin, G. Numerical modeling of slippage and adsorption effects on gas transport in shale formations using the lattice Boltzmann method. *Journal of Natural Gas Science and Engineering* **2015**, *26*, 345–355.

(5) Soulaine, C.; Creux, P.; Tchelepi, H. A. Micro-continuum Framework for Pore-Scale Multiphase Fluid Transport in Shale Formations. *Transport in Porous Media* **2018**, *127*, 85–112.

(6) Neimark, A. V.; Vishnyakov, A. Phase Transitions and Criticality in Small Systems: Vapor-Liquid Transition in Nanoscale Spherical Cavities. *The Journal of Physical Chemistry B* **2006**, *110*, 9403–9412.

(7) Firouzi, M.; Wilcox, J. Molecular modeling of carbon dioxide transport and storage in porous carbon-based materials. *Microporous and Mesoporous Materials* **2012**, *158*, 195–203.

(8) Striolo, A.; Gubbins, K. E.; Gruszkiewicz, M. S.; Cole, D. R.; Simonson, J. M.;

Chialvo, A. A.; Cummings, P. T.; Burchell, T. D.; More, K. L. Effect of Temperature on the Adsorption of Water in Porous Carbons. *Langmuir* **2005**, *21*, 9457–9467.

(9) Wang, J.; Kang, Q.; Chen, L.; Rahman, S. S. Pore-scale lattice Boltzmann simulation of micro-gaseous flow considering surface diffusion effect. *International Journal of Coal Geology* **2017**, *169*, 62–73.

(10) Mehmani, A.; Prodanović, M.; Javadpour, F. Multiscale, Multiphysics Network Modeling of Shale Matrix Gas Flows. *Transport in Porous Media* **2013**, *99*, 377–390.

(11) Clarkson, C. R.; Nobakht, M.; Kaviani, D.; Ertekin, T. Production analysis of tight-gas and shale-gas reservoirs using the dynamic-slippage concept. *SPE Journal* **2012**, *17*, 230–242.

(12) Firouzi, M.; Wilcox, J. Slippage and viscosity predictions in carbon micropores and their influence on CO2 and CH4 transport. *The Journal of Chemical Physics* **2013**, *138*, 064705.

(13) Sinha, S.; Braun, E.; Determan, M.; Passey, Q.; Leonardi, S.; Boros, J.; Wood III, A.; Zirkle, T.; Kudva, R. Steady-state permeability measurements on intact shale samples at reservoir conditions-effect of stress, temperature, pressure, and type of gas. *SPE Middle East Oil and Gas Show and Conference* **2013**, 956–970.

(14) Ortiz-Young, D.; Chiu, H.-C.; Kim, S.; Voïtchovsky, K.; Riedo, E. The interplay between apparent viscosity and wettability in nanoconfined water. *Nature Communications* **2013**, *4*, 1–6.

(15) Collell, J.; Ungerer, P.; Galliero, G.; Yiannourakou, M.; Montel, F.; Pujol, M. Molecular Simulation of Bulk Organic Matter in Type II Shales in the Middle of the Oil Formation Window. *Energy & Fuels* **2014**, 7457–7466.

(16) Bousige, C.; Ghimbeu, C. M.; Vix-Guterl, C.; Pomerantz, A. E.; Suleimenova, A.; Vaughan, G.; Garbarino, G.; Feygenson, M.; Wildgruber, C.; Ulm, F.-J.; *et al.*, Realistic molecular model of kerogen's nanostructure. *Nature Materials* **2016**, *15*, 576–582.

(17) Atmani, L.; Bichara, C.; Pellenq, R. J.-M.; Van Damme, H.; van Duin, A. C. T.; Raza, Z.; Truflandier, L. A.; Obliger, A.; Kralert, P. G.; Ulm, F. J.; Leyssale, J.-M. From cellulose to kerogen: molecular simulation of a geological process. *Chemical Science* **2017**, *8*, 8325–8335.

(18) Vasileiadis, M.; Peristeras, L. D.; Papavasileiou, K. D.; Economou, I. G. Modeling of Bulk Kerogen Porosity: Methods for Control and Characterization. *Energy & Fuels* **2017**, *31*, 6004–6018.

(19) Obliger, A.; Valdenaire, P.-L.; Capit, N.; Ulm, F. J.; Pellenq, R. J.-M.; Leyssale, J.-M. Poroelasticity of Methane-Loaded Mature and Immature Kerogen from Molecular Simulations. *Langmuir* **2018**, *34*, 13766–13780.

(20) Zhang, H.; Ahmed, M.; Zhan, J. Recent advances in molecular simulation of oil shale kerogen. *Fuel* **2022**, *316*, 123392.

(21) Obliger, A.; Bousige, C.; Coasne, B.; Leyssale, J.-M. Development of Atomistic Kerogen Models and Their Applications for Gas Adsorption and Diffusion: A Mini-Review. *Energy & Fuels* **2023**, *37*, 1678–1698.

(22) Coasne, B.; Gubbins, K. E.; Pellenq, R. J.-M. Temperature effect on adsorption/desorption isotherms for a simple fluid confined within various nanopores. *Adsorption* **2005**, *11*, 289–294.

(23) Pikunic, J.; Llewellyn, P.; Pellenq, R.; Gubbins, K. E. Argon and nitrogen adsorption in disordered nanoporous carbons: Simulation and experiment. *Langmuir* **2005**, *21*, 4431–4440.

(24) Billemont, P.; Coasne, B.; Weireld, G. D. Adsorption of carbon dioxide, methane, and their mixtures in porous carbons: Effect of surface chemistry, water content, and pore disorder. *Langmuir* **2013**, *29*, 3328–3338.

(25) Collell, J.; Galliero, G.; Gouth, F.; Montel, F.; Pujol, M.; Ungerer, P.; Yiannourakou, M. Molecular simulation and modelisation of methane/ethane mixtures adsorption onto a microporous molecular model of kerogen under typical reservoir conditions. *Microporous Mesoporous Materials* **2014**, *197*, 194–203.

(26) Falk, K.; Pellenq, R.; Ulm, F. J.; Coasne, B. Effect of Chain Length and Pore Accessibility on Alkane Adsorption in Kerogen. *Energy & Fuels* **2015**, *29*, 7889–7896.

(27) Ho, T. A.; Wang, Y.; Criscenti, L. J. Chemo-mechanical coupling in kerogen gas adsorption/desorption. *Physical Chemistry Chemical Physics. PCCP* **2018**, *20*, 12390–12395.

(28) Huang, L.; Ning, Z.; Wang, Q.; Zhang, W.; Cheng, Z.; Wu, X.; Qin, H. Effect of organic type and moisture on CO2/CH4 competitive adsorption in kerogen with implications for CO2 sequestration and enhanced CH4 recovery. *Applied Energy* **2018**, *210*, 28–43.

(29) Liu, J.; Xi, S.; Chapman, W. G. Competitive sorption of CO2 with gas mixtures in nanoporous shale for enhanced gas recovery from density functional theory. *Langmuir* **2019**, *35*, 8144–8158.

(30) Alafnan, S.; Solling, T.; Mahmoud, M. Effect of kerogen thermal maturity on methane adsorption capacity: A molecular modeling approach. *Molecules* **2020**, *25*, 3764.

(31) Babatunde, K. A.; Negash, B. M.; Mojid, M. R.; Ahmed, T. Y.; Jufar, S. R. Molecular simulation study of CO2/CH4 adsorption on realistic heterogeneous shale surfaces. *Appl. Surf. Sci.* **2021**, *543*, 148789.

(32) Chang, C.; Zhang, J.; Hu, H.; Zhang, D.; Zhao, Y. Molecular simulation of adsorption in deep marine shale gas reservoirs. *Energies* **2022**, *15*, 944.

(33) Falk, K.; Coasne, B.; Pellenq, R.; Ulm, F.-J.; Bocquet, L. Subcontinuum mass transport of condensed hydrocarbons in nanoporous media. *Nature communications* **2015**, *6*, 6949.

(34) Collell, J.; Galliero, G.; Vermorel, R.; Ungerer, P.; Yiannourakou, M.; Montel, F.; Pujol, M. Transport of Multicomponent Hydrocarbon Mixtures in Shale Organic Matter by Molecular Simulations. *Journal of Physical Chemistry C* **2015**, *119*.

(35) Obliger, A.; Pellenq, R.; Ulm, F.-J.; Coasne, B. Free Volume Theory of Hydrocarbon Mixture Transport in Nanoporous Materials. *The Journal of Physical Chemistry Letters* **2016**, *7*, 3712–3717, PMID: 27570884.

(36) Obliger, A.; Ulm, F.-J.; Pellenq, R. J.-M. Impact of Nanoporosity on Hydrocarbon Transport in Shales' Organic Matter. *Nano Letters* **2018**, *18*, 832 – 837.

(37) Sun, Z.; Li, X.; Liu, W.; Zhang, T.; He, M.; Nasrabadi, H. Molecular dynamics of methane flow behavior through realistic organic nanopores under geologic shale condition: Pore size and kerogen types. *Chemical Engineering Journal* **2020**, *398*, 124341.

(38) Liu, J.; Zhao, Y.; Yang, Y.; Mei, Q.; Yang, S.; Wang, C. Multicomponent shale oil flow in real kerogen structures via molecular dynamic simulation. *Energies* **2020**, *13*, 3815.

(39) Alafnan, S.; Falola, Y.; Mansour, O. A.; Al Samadony, K.; Awotunde, A.; Aljawad, M. Enhanced recovery from organic-rich shales through carbon dioxide injection: Molecular-level investigation. *Energy Fuels* **2020**, *34*, 16089–16098.

(40) Xu, H.; Yu, H.; Fan, J.; Xia, J.; Wang, F.; Wu, H. Enhanced gas recovery in kerogen pyrolytic pore network: Molecular simulations and theoretical analysis. *Energy Fuels* **2021**, *35*, 2253–2267.

(41) Afagwu, C.; Al-Afnan, S.; Patil, S.; Aljaberi, J.; Mahmoud, M. A.; Li, J. The impact of pore structure and adsorption behavior on kerogen tortuosity. *Fuel* **2021**, *303*, 121261.

(42) Thyagarajan, R.; Sholl, D. S. Molecular simulations of CH4 and CO2 diffusion in rigid nanoporous amorphous materials. *Journal of Physical Chemistry C* **2022**, *126*, 8530–8538.

(43) Sun, Z.; Huang, B.; Li, Y.; Lin, H.; Shi, S.; Yu, W. Nanoconfined methane flow behavior through realistic organic shale matrix under displacement pressure: a molecular simulation investigation. *Journal of Petroleum Exploration and Production Technology* **2022**, *12*, 1193–1201.

(44) Obliger, A.; Valdenaire, P.-L.; Ulm, F.-J.; Pellenq, R. J.-M.; Leyssale, J.-M. Methane Diffusion in a Flexible Kerogen Matrix. *The Journal of Physical Chemistry B* **2019**, *123*, 5635–5640.

(45) Ariskina, K.; Galliéro, G.; Obliger, A. Free Volume Model for Transport in Flexible Kerogen of Source Rock's Organic Matter. *The Journal of Physical Chemistry B* **2022**, *126*, 7409–7417.

(46) Wang, Z.; Li, Y.; Liu, H.; Zeng, F.; Guo, P.; Jiang, W. Study on the adsorption, diffusion and permeation selectivity of shale gas in organics. *Energies* **2017**, *10*, 142.

(47) Sui, H.; Zhang, F.; Wang, Z.; Wang, D.; Wang, Y. Effect of kerogen maturity, water content for carbon dioxide, methane, and their mixture adsorption and diffusion in kerogen: A computational investigation. *Langmuir* **2020**, *36*, 9756–9769.

(48) Yang, Y.; Narayanan Nair, A. K.; Sun, S. Sorption and Diffusion of Methane and Carbon Dioxide in Amorphous Poly(alkyl acrylates): A Molecular Simulation Study. *The Journal of Physical Chemistry B* **2020**, *124*, 1301–1310.

(49) Descallar, F. B. A.; Matsukawa, S. *NMR and MRI of Gels*; New Developments in NMR; The Royal Society of Chemistry, 2020; Chapter 3, pp 89–109.

(50) Majer, G.; Southan, A. Adenosine triphosphate diffusion through poly(ethylene glycol) diacrylate hydrogels can be tuned by cross-link density as measured by PFG-NMR. *The Journal of Chemical Physics* **2017**, *146*, 225101.

(51) Fujita, H. Notes on Free Volume Theories. *Polymer Journal* **1991**, *23*, 1499–1506.

(52) Fujita, H. Free volume interpretation of the polymer effect on solvent dynamics. *Macromolecules* **1993**, *26*, 643–646.

(53) Harris, J. G.; Yung, K. H. Carbon Dioxide's Liquid-Vapor Coexistence Curve And Critical Properties as Predicted by a Simple Molecular Model. *The Journal of Physical Chemistry* **1995**, *99*, 12021–12024.

(54) Martyna, G. J.; Tuckerman, M. E.; Tobias, D. J.; Klein, M. L. Explicit reversible integrators for extended systems dynamics. *Molecular Physics* **1996**, *87*, 1117–1157.

(55) Ismail, A. F.; Khulbe, K. C.; Matsuura, T. Gas separation membranes. *Switz. Springer* **2015**, *10*, 973–978.